Annals of Nuclear Energy 197 (2024) 110237

Contents lists available at ScienceDirect

Annals of Nuclear Energy

journal homepage: www.elsevier.com/locate/anucene

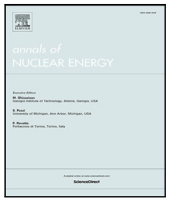

On the need for multi-dimensional models for the safety analysis of (fast-spectrum) Molten Salt Reactors

Nahom Habtemariam [a,b,c,*], Carlo Fiorina [a], Stefano Lorenzi [b], Antonio Cammi [b]

[a] Texas A&M University, College Station, TX, 77840, United States of America
[b] Politecnico di Milano, Department of Energy, CeSNEF-Nuclear Engineering Division, Nuclear Reactors Group, via La Masa, 34, Milano, 20156, Italy
[c] École polytechnique fédérale de Lausanne, Laboratory for Reactor Physics and Systems Behaviour, Lausanne, 1015, Switzerland

ARTICLE INFO

Keywords:
Molten salt fast reactor (MSFR)
Safety analysis
Multi-physics simulation

ABSTRACT

This paper aims at characterizing the impact of adopting numerical models with different dimensionalities on the predicted behavior of fast-spectrum Molten Salt Reactors (MSRs). The study encompasses 1-D, 2-D, and 3-D representations of thermal-hydraulics and precursor transport/diffusion, along with spatial and point kinetics models for neutronics. We evaluate the accuracy of each model based on steady-state results and on the reactor response to 2 different transient initiators. The findings emphasize the significance of utilizing a 3-D representation with accurate thermal-hydraulics modeling, and with either spatial kinetics or carefully calibrated point kinetics incorporating a spatial description of precursors transport. 2-D and 1-D models can reproduce main trends and remain valuable tools for e.g. reactor design, control-oriented studies or uncertainty quantification. However, proper calibration of these models is needed and the user should be aware that alterations in flow patterns could jeopardize model calibration and hide first-order local effects.

1. Introduction

The importance of employing multi-dimensional tools for the modeling of Molten Salt Reactors (MSRs) was already recognized during the Molten Salt Reactor Project at the Oak Ridge National Laboratory. For instance, Ball and Kerlin (1965) developed a model for the stability analysis of the Molten Salt Reactor Experiment where the core was divided into radial and axial regions to accurately account for different neutron importance and the transport of delayed neutron precursors. The renewed interest in MSRs in the early 2000s led to the development of several new codes capable of simulating a liquid and circulating fuel. Tools like DYN-1D and DYN-3D were developed as part of the EURATOM MOST project, further emphasizing the significance of spatial representation of the MSR core (Křepel et al., 2007). Approximately a decade later, several studies in the frame of the EURATOM EVOL project focused on the need for multi-dimensional and even multi-scale simulations of thermal-spectrum MSRs (Zanetti et al., 2015).

Most of the activities on the modeling and simulation of fast-spectrum MSRs started in the early 2010s. Building on the experience gained from thermal MSRs, the community aimed immediately at multi-dimensional models. OpenFOAM has been one of the first tools that has been used to develop dedicated codes for fast-spectrum MSRs (Aufiero et al., 2014b; Fiorina et al., 2015; Cervi et al., 2019). These codes still represent a reference choice for several institutions, especially in Europe. Similar studies have also been conducted using different tools, including COMSOL (Fiorina et al., 2014) and some in-house codes (see Tiberga et al., 2020). In the US, tools for MSRs have been developed for instance based on the MOOSE framework (Yang et al., 2022; Lindsay et al., 2018) and on the GOTHIC software package (Harvill et al., 2022).

These tools have been developed to overcome limitations that legacy LWR-oriented codes have for the modeling of complex geometries, volumetric heat generation, transport of delayed neutron precursors, and the tight coupling between the physics governing the system. Although the need for multi-dimensional tools for the modeling of fast-spectrum MSRs is generally acknowledged in the community, we have not found dedicated studies that systematically quantifies the effect of dimensionality on the modeling of these systems. Such an analysis plays a crucial role in the modeling of fast-spectrum MSRs for several reasons. Firstly, it can provide valuable insights into the limitations of low-dimensional models. Secondly, based on this analysis, one can select the appropriate model for each specific application. Lastly, it can facilitate the development of informed low-dimensional models, such as NQA-1 codes for licensing purposes, by utilizing the information derived from high-dimensional models.

* Corresponding author at: Texas A&M University, College Station, TX, 77840, United States of America.
E-mail address: nahom.habtemariam@tamu.edu (N. Habtemariam).

https://doi.org/10.1016/j.anucene.2023.110237
Received 21 July 2023; Received in revised form 20 October 2023; Accepted 8 November 2023
Available online 22 November 2023
0306-4549/© 2023 The Author(s). Published by Elsevier Ltd. This is an open access article under the CC BY license (http://creativecommons.org/licenses/by/4.0/).

This study aims at provide a systematic comparison between the results obtained using 1-D, 2-D, and 3-D geometries, as well as using spatial or point neutron kinetics (Mattioli et al., 2021). The reference geometry chosen for this analysis is the Molten Salt Fast Reactor (MSFR). At steady-state, we focus both on thermal-hydraulics results and on the effective delayed neutron fraction in circulating condition (β_{circ}). In addition to significantly impacting the reactor behavior, β_{circ} is a good indicator of the effect of dimensionality, since it is affected by both the distribution of delayed neutron precursors, and hence by the thermal hydraulics, and by neutron importance weighting. Regarding transient behavior, we compare the prediction of different models for two different transient scenarios: reactivity insertion and loss of flow. In evaluating the effect of dimensionality, we use the 3-D diffusion-based model as a reference, since neutron diffusion is known to provide good results for the MSFR (Fiorina et al., 2012). We exclude from the analyses a fully lumped 0-D model since it is known to yield inaccurate results.[1]

2. Computational tools and methods

GeN-Foam (Fiorina et al., 2015; Fiorina, 2022), an OpenFOAM-based multi-physics solver for nuclear applications, has been used for this work. GeN-Foam includes three different sub-solvers for thermal-hydraulics (one- or two-phase), neutronics and thermal-mechanics, and has the ability to model circulating fuel reactors. For this work, only the thermal-hydraulics and neutronics sub-solver have been used. The thermal-hydraulics sub-solver employs a PISO-SIMPLE algorithm to solve the Navier–Stokes equations, whereas the steady state neutronics problem is solved using a power iteration scheme. The time integration is performed with a first order implicit Euler scheme. The coupling between the equations in each sub-solver is achieved using Picard iteration.

2.1. Thermal-hydraulics

GeN-Foam makes use of a standard cell-centered finite-volume formulation of the Reynolds-Averaged Navier Stokes equations, but extended for the treatment of complex components such as the core and heat exchangers using a porous medium approach. These are the resulting equations in the case of single-phase simulations:

$$\frac{\partial \gamma \rho}{\partial t} + \nabla \cdot (\gamma \rho \mathbf{u}) = 0 \tag{1}$$

$$\frac{\partial \gamma \rho \mathbf{u}}{\partial t} + \nabla \cdot (\gamma \rho \mathbf{u} \otimes \mathbf{u}) = \nabla \cdot (\mu_T \nabla \mathbf{u}) - \nabla \gamma p + p_i \nabla \gamma + \gamma \mathbf{F_g} + \gamma \mathbf{F_{ss}} \tag{2}$$

$$\frac{\partial \gamma \rho e}{\partial t} + \nabla \cdot (\mathbf{u} \gamma (\rho e + p)) = \nabla \cdot (\gamma k_T \nabla T) + \gamma \mathbf{F_{ss}} \cdot \mathbf{u} + \gamma \dot{Q_{ss}} \tag{3}$$

In these equations, the fraction of the volume occupied by the fluid is represented by γ and it is usually referred to as porosity. The terms $\mathbf{F_{ss}}$ and Q_{ss} account for the interaction between fluid and the sub-scale structures. In practice, they are calculated using correlations for friction factors and Nusselt numbers, which makes the solution in porous regions similar to that obtained using sub-channel codes.[2] When all the volume is occupied by the fluid, the Eqs. (1), (2), (3) revert to the standard RANS equations. Consequently, the same set of equations are used throughout the mesh, which avoids the need for coupling the equations at the interfaces between porous and clear-fluid zones. The $k-\epsilon$ turbulence model is adopted in clear-fluid regions while k and ϵ are forced to their equilibrium values in porous regions. These equilibrium values are calculated based on dedicated correlations (see Fiorina et al., 2015 for details).

[1] A 0-D approach for temperature or neutron precursors would require either to the set the core outlet equal to the average value, or to calculate it based on inlet and average value. The first approach is fundamentally inaccurate, while the second leads to nonphysical oscillations in the solution.

[2] One can prove that sub-channel methods are a special case of porous-medium methods (Todreas et al., 2021).

2.2. Neutronics

GeN-Foam allows to chose from a variety of neutronics models. In this work, we will make use of the diffusion, adjoint-diffusion and point-kinetics models.

2.2.1. Diffusion solver

The diffusion model solves for the following standard set of equations:

$$\begin{aligned}\frac{1}{v_g}\frac{\partial \phi_g}{\partial t} = {} & \nabla \cdot D \nabla \phi_g - \Sigma_{r,g}\phi_g + \\ & + \frac{(\nu\Sigma_f)_g}{k_{eff}}(1-\beta)\chi_{p,g}\phi_g + S_{n,g}(1-\beta)\chi_{p,g} \\ & + S_d \chi_{d,g} + S_{s,g}\end{aligned} \tag{4}$$

$S_{n,g}$, S_d, $S_{s,g}$ account for neutron sources coming from, respectively, other fissions in other energy groups, delayed neutron precursors, and the scattering source from other energy groups:

$$S_{n,g} = \frac{1}{k_{eff}} \sum_{j \neq g} (\nu\Sigma_f)_j \phi_j \tag{5}$$

$$S_d = \sum_k \lambda_k c_k \tag{6}$$

$$S_{s,g} = \sum_{j \neq g} \Sigma_{s,j \to g} \phi_j \tag{7}$$

The standard precursors equation is adapted to the modeling of circulating-fuel systems as:

$$\begin{aligned}\frac{\partial C_i}{\partial t} + u \cdot \nabla C_i = {} & -\lambda_i C_i + \\ & + \beta_i \sum_{g=1}^{G} \frac{(\nu\Sigma_f)_g}{k_{eff}} \phi_g + \nabla \cdot D_i \nabla C_i\end{aligned} \tag{8}$$

The diffusion sub-solver allows to perform both eigenvalue and transient calculations. For more details, the interested reader can refer to Fiorina et al. (2016).

2.2.2. Adjoint diffusion solver

The adjoint diffusion model solves for the following standard set of equations:

$$\begin{aligned}\nabla \cdot D_i \nabla \phi_i^* - \Sigma_{r,i}\phi_i^* + \sum_{j \neq i} \Sigma_{s,i \to j}\phi_i^* + \\ + \frac{1-\beta}{k_{eff}}(\nu\Sigma_f)_i \sum_{i'=1}^{G} \chi_{p,i'}\phi_{i'}^* + \frac{(\nu\Sigma_f)_i}{k_{eff}} \sum_{k=1}^{R} \beta_k C_k^* = 0\end{aligned} \tag{9}$$

$$-\nabla \cdot (-\mathbf{u} C_k^*) + \nabla \cdot \frac{\nu_T}{Sc_T} \nabla C_k^* - \lambda_k C_k^* + \lambda_k \sum_{i=1}^{G} \chi_{d,i}\phi_i^* = 0 \tag{10}$$

where ϕ_i^* is the adjoint flux of the ith group. C_k^* is the importance of a delayed neutron precursor.

2.2.3. Point-kinetics solver

A hybrid approach is adopted in the GeN-Foam point-kinetics solver for liquid systems. The power is described as usual in a lumped manner, as in the classic point-kinetics equation, but the equations for precursors concentration are solved in both space and time. The delayed neutron source appearing in the power equation is obtained via a weighted integral of the delayed neutron precursors concentrations over the volume of the reactor. Details of the derivation can be found in Mattioli et al. (2021), with the resulting equations that reads as:

$$\frac{dP}{dt} = \frac{\rho(t) - \beta_{eff}}{\Lambda} P(t) + \sum_{i=1}^{R} \lambda_i \hat{C}_i(t) \tag{11}$$

$$\frac{\partial \tilde{c}_i(r,t)}{\partial t} + u \cdot \nabla \tilde{c}_i(r,t) = -\lambda \tilde{c}_i(r,t) + \frac{\beta_i P(t)}{\Lambda} S(r,t) + \nabla \cdot D_i \nabla \tilde{c}_i(r,t) \tag{12}$$

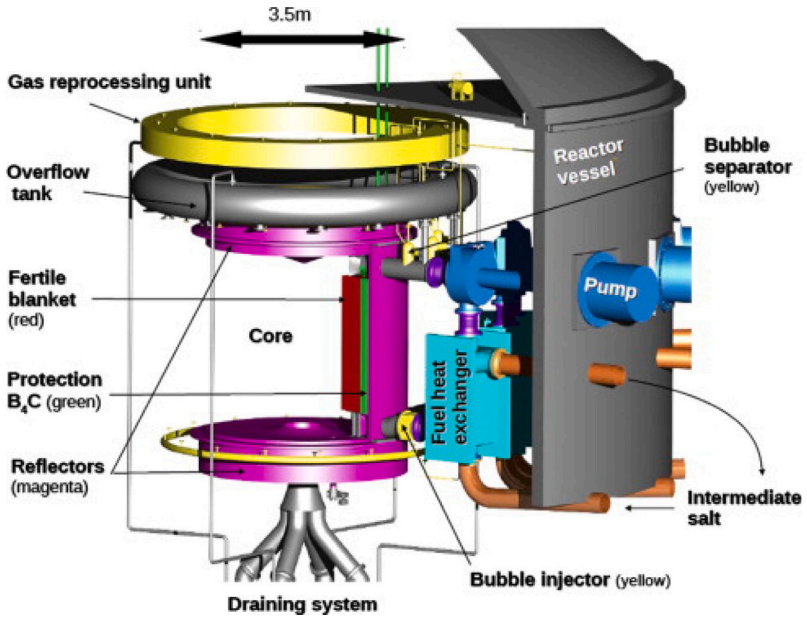

Fig. 1. MSFR conceptual scheme.

$$\hat{C}_i(t) = \frac{\int_V W(r)\tilde{c}_i(r,t)dV}{\int_V W(r)S(r)dV} \tag{13}$$

where $W(r)$ is the weight function (usually the adjoint flux).

In order to allow for a consistent comparison between diffusion-based and point-kinetics-based results, the kinetic parameters required by the point-kinetics model (Λ, β and feedback coefficients) were calculated from the steady state results of the forward and adjoint diffusion solvers in a 3-D geometry.

It is worth pointing out that the solution of Eqs. (11) and (12) requires a specific procedure of initialization. In the case of solid-fuel reactors, the point-kinetics equations can be easily initialized by imposing a target initial power and by solving the steady state equations to find the initial values of the precursors. On the other hand, in the case of Eqs. (11) and (12), one has to first solve for the precursors equations to determine the precursors spatial distributions. Based on these distributions, one can then use Eq. (13) to calculate the precursor source term in the power equation. Finally, the solution of the steady-state equation for power allows deriving that, at equilibrium, the following condition must apply:

$$\rho_{eq} = \beta_{eff} - \frac{\Lambda \sum_{i=1}^{R} \lambda_i \hat{C}_i(0)}{P_0} \tag{14}$$

This means that the overall reactivity during the simulation must be expressed as the sum of the usual terms associated with feedback coefficients and control rods, with the addition ρ_{eq}:

$$\rho(t) = \rho_{feedback} + \rho_{control\,Rods} + \rho_{eq} \tag{15}$$

The new term ρ_{eq} represents the reactivity loss associated to the circulation of delayed neutron precursors. As an alternative formulation, one can substitute Eq. (15) into the power equation and redefine $\rho(t) = \rho_{feedback} + \rho_{control\,Rods}$ to obtain:

$$\frac{dP(t)}{dt} = \frac{\rho(t) - \beta_{circ}}{\Lambda} P(t) + \sum_{i=1}^{R} \lambda_i \hat{C}_i(t) \tag{16}$$

where the new term

$$\beta_{circ} = \frac{\Lambda \sum_{i=1}^{R} \lambda_i \hat{C}_i(t)(0)}{P_0} \tag{17}$$

represents the effective (reduced) β that is determined by the circulation of the delayed neutron precursors.

Fig. 2. MSFR 1-D geometry and mesh.

3. Computational models

All the MSFR models in this paper are made of core, hot leg, cold leg, heat exchanger and pump (Fig. 1). The effects of both heat exchanger and pump on the fluid flow are described using the source and sink terms in Eqs. (3) and (2). The pump is modeled as a distributed momentum source in a specific region, whereas the heat exchanger is represented by both a momentum sink (pressure drop) and a heat sink. The analysis is restricted to the primary circuit only, with the heat exchanger that is modeled as a fixed-temperature heat sink.

The main reactor parameters are listed in Table 3, whereas the thermo-physical properties are given in Table 4. Three different geometries are employed, as shown in Figs. 4, 3, 2:

- A **1-D model** consisting of a channel. Cyclic boundary conditions applied on the top and bottom edges are used to model the re-circulation in the closed loop characterizing the primary system of the MSFR.
- A **2-D axial-symmetric model**, often used within the MSFR community and constituting a more detailed and realistic representation of the MSFR primary circuit.
- A **3-D model** describing one-sixteenth of the full core.

It can be useful to point out that moving from a 3-D to a 2-D representation of the core implies compromising on the fidelity of the representation, as it is normally impossible to maintain simultaneously the same inlet velocities, entry area, entry angle, vessel curvature, etc. One should expect potentially different flow fields, with non-negligible impacts on other quantities such as temperature and precursors concentrations, as discuss below. In our case, we employed realistic 2-D and 3-D geometries that have both been used in the frame of the EURATOM EVOL, SAMOFAR, and SAMOSAFER projects.

Three different neutronics model have been employed to extend the investigation about the impact of dimensionality to the dimensionality of the equations themselves:

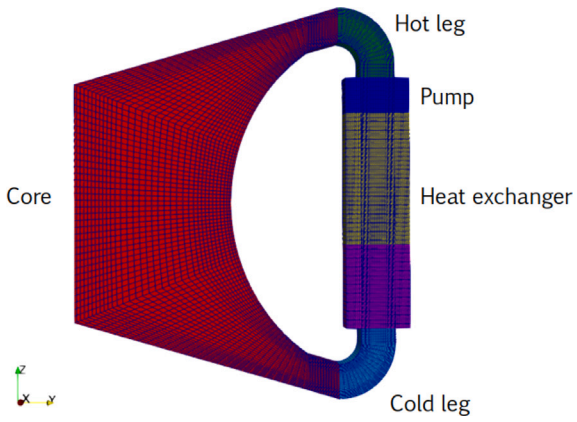

Fig. 3. MSFR 2-D geometry and mesh.

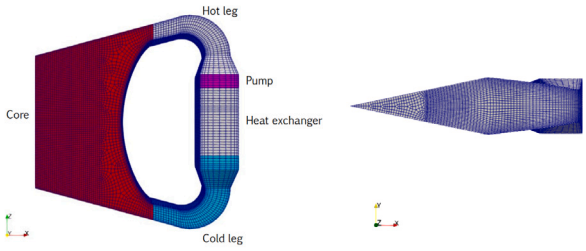

(a) (b)

Fig. 4. MSFR 3-D geometry and mesh: (a) side view and (b) top view.

Table 1
Energy group structures for the multi-group diffusion calculation.

Energy group	Energy upper boundary (MeV)
1	7.485×10^{-4}
2	5.531×10^{-3}
3	2.479×10^{-2}
4	4.979×10^{-1}
5	2.231
6	20

- **Spatial kinetics** using multi-group diffusion equation, 6 energy groups (Fiorina et al., 2012), and 8 delayed neutrons groups. The group structures are given in Tables 1 and 2. Albedo boundary conditions are used in the 2-D and 3-D models to account for the presence of reflector and blanket.
- **Point-kinetics informed by the steady state diffusion results**. In this case, the results of a diffusion calculation are used to determine power shape and neutron importance, where the latter is approximated by the scalar flux.
- **Point-kinetics without a spatial shape function and weighting field.** Although this model is simplistic, it represents a useful lower limit to the achievable fidelity in a multi-physics context. It is worth to point out that a flat spatial shape function affects the prediction of delayed neutrons precursors distribution since the shape function $S(r,t)$ appears in the source term in Eq. (12).

Point-kinetics parameters have been calculated based on the 3-D geometry and using diffusion results for the forward and adjoint flux. The prompt generation time has been calculated based on the following definition (Bell and Glasstone, 1970):

$$\Lambda = \frac{1}{F}\int_{V,E} \phi^* \phi dV dE = \frac{\int_V \sum_{g=1}^{G} \phi_g^* \phi_g}{\sum_{g=1}^{G} \int_V \phi_g^* (\chi_g (1-\beta) + \sum_{i=1}^{R} \chi_{g,i}\beta_i)(\nu\Sigma_{eff})'_g \phi'_g dV} \quad (18)$$

The result is 7.57×10^{-7} s.

Temperature coefficients are calculated by computing k_{eff} in two distinct situations. One refers to the steady-state nominal condition and the other to the steady state condition with an increase of 10% in thermal power. In order to separate the effect of temperature and density, the density was kept fixed. The reactivity change corresponds to:

$$\Delta\rho = \frac{k_{nominal} - k_{highPower}}{k_{highPower} k_{nominal}} \quad (19)$$

The reactivity feedback coefficient due to Doppler effect is usually evaluated in fast reactors assuming a logarithmic dependence of the reactivity on the fuel temperature, which gives rise to the definition of the Doppler constant:

$$K_D = \frac{\Delta\rho}{\ln \frac{T_{eff,2}}{T_{eff,1}}} \quad (20)$$

where T_{eff} is the effective temperature in the core, which is used to feed the point-kinetics equations for computing the term $\rho_{feedback}$ as in

Table 2
Delayed neutrons precursors data for the eight groups employed in this work.

Precursors group	β_0 (pcm)	Decay constant (s^{-1})
1	22.2	1.247×10^{-2}
2	48.1	2.829×10^{-2}
3	40.5	4.252×10^{-2}
4	64.5	1.330×10^{-1}
5	102.1	2.925×10^{-1}
6	17.7	6.665×10^{-1}
7	22.3	1.635
8	5.1	3.555

Table 3
Key parameters for the steady-state simulations. The momentum source of the pump is set in order to match the nominal mass flow rate (1180 kg/s per sector). The volumes and the power given below correspond to the 3D and 1D model, that represent one sector of the entire reactor (composed of 16 sectors). The 2D model is a fraction of a sector (1/10th), therefore the volumes and power are scaled accordingly.

	Parameters	Value
Core	Volume	0.56 m^3
	Total power	187.5 MW
Hot leg/cold leg	Volume	0.14 m^3
Heat exchanger	Volume	0.20 m^3
	Heat transfer coefficient	2×10^4 W/m^2 K
	Volumetric area	912 m^{-1}
	Temperature sink	908 K
	Height wrt core	0 m
Pump	Volume	0.04 m^3

Table 4
Thermo-physical properties of the fuel salt evaluated at 973 K (Brovchenko et al., 2019).

Parameter	Value
Kinematic viscosity	0.01 m^2/s
Expansion coefficient	2.14×10^{-4}
Prandtl number	16
Specific heat	1594 J/kg K
Density	4125 kg/m^3

Table 5
Maximum, minimum and average temperature in the core.

	T_{max} (K)	T_{min} (K)	T_{av} (K)
1D	1023.7	924.5	975.7
2D	1121.4	919.2	964.8
3D	1184.5	922.7	977.0

Section 2.2.3. This quantity is computed as[3]:

$$T_{eff} = \frac{\int_V \phi^*(r)T(r)\phi(r)dV}{\int_V \phi^*(r)\phi(r)dV} \simeq \frac{\int_V T(r)\phi^2(r)dV}{\int_V \phi^2(r)dV} \quad (21)$$

It is worth pointing out that we observed only a 2% difference in Doppler effect when we used 2 different uniform temperatures instead of realistic temperature profiles obtained by steady-state simulations at different powers. This provides confidence that temperature weighting allows capturing the effect of neutron importance in the reactor. On the other hand, without importance weighting, one would obtain very different Doppler coefficients (α_T) of 4.0 pcm/K and 4.72 pcm/K for the case of uniform and realistic temperatures, respectively.

For the density feedback, similar considerations can be made in terms of weighting the density field. The density coefficient has then been evaluated as:

$$\alpha_d = \frac{\Delta\rho}{d_{eff,highPower} - d_{eff,nominal}} \quad (22)$$

where d_{eff} is evaluated based on an expression similar to (21).

Similar results can be obtained for the density coefficient, with the additional caveat that this effect is strictly related to neutron leakage: a 2-D geometry will provide a certain degree of inaccuracy while a 1-D geometry is simply not suitable to evaluate density feedback effects. Only density and Doppler feedback coefficients are considered in this work, since core thermal expansion effects are known to be normally negligible for the MSFR (Fiorina et al., 2013).

4. Steady-state results

To obtain a steady-state result for the 3 geometries, an eigenvalue calculation coupled with the thermal-hydraulics solver has been run. The multi-group neutron diffusion model was used for this purpose.[4] The steady state flow fields in the core are displayed in Figs. 5(a) and 5(b) for the 2-D and 3-D case, respectively. It can be observed that the 2-D case predicts smaller low-velocity regions close to the top and bottom reflectors, towards the core symmetry axis. Of course, the 1-D model cannot predict regions with lower velocities or the risk of flow detachment, and its results are not reported for brevity. We observe that a modeling and simulation specialist could improve the results of the 2-D case by performing a 3-D simulation first, and fine-tuning the geometry of the 2-D case. However, the non-linear nature of the Navier–Stokes equations makes it very difficult to obtain a 2-D geometry that is fully representative of a 3-D case, notably for varying flow rates.

The differences in flow fields lead to important differences in temperature and delayed neutron precursor concentrations. Temperature distributions are given in Figs. 6–8, while total precursors concentrations are reported in Figs. 9–11. Some quantities of interest are summarized in Table 5. While the minimum and average temperatures do not differ significantly, the maximum temperature in the 1-D model is approximately 100 K less than the 2-D case, and about 160 K less than the 3-D case. As mentioned, this is associated with the fact that the 1-D is not able to reproduce the existence of low-velocity (stagnation, re-circulation) regions in the core. The 2-D case can reproduce qualitatively the results of a 3-D case but results show that local quantities can significantly differ. In our case, low-velocity regions are clearly visible near the central axis of the core, both at the bottom and at the top.

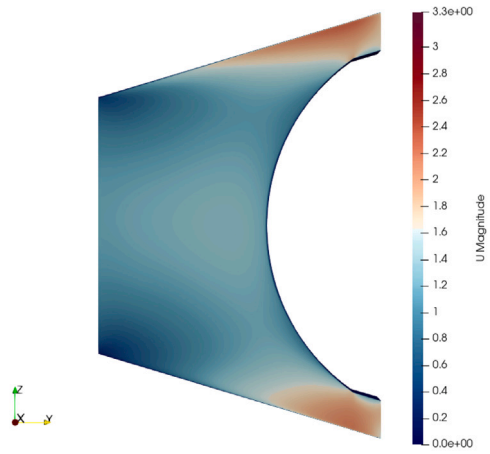

(a) Velocity magnitude on the 2-D geometry

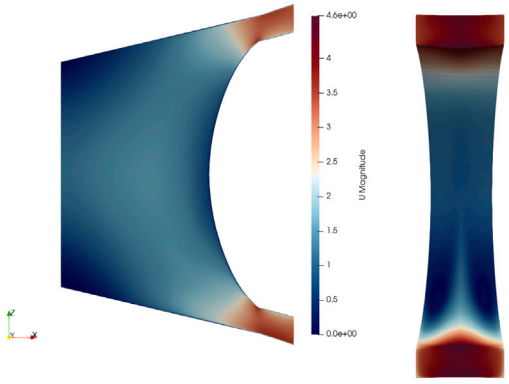

(b) Velocity magnitude on the symmetry plane for the 3D geometry

Fig. 5. Velocity magnitude fields for the 2-D geometry(a) and the 3-D geometry(b).

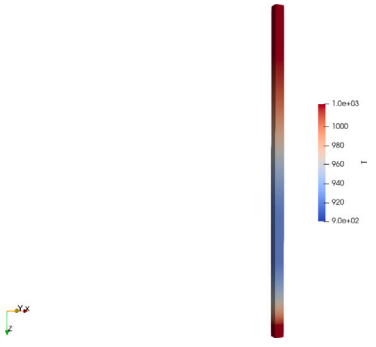

Fig. 6. Temperature distribution for the 1-D geometry.

4.1. Effective delayed neutron fraction in circulating conditions

The value of the circulating delayed neutron fraction has been determined at different flow rates in order to gain insights in the

[3] The adjoint flux ($\phi^*(r)$) is assumed as equal to the forward flux ($\phi(r)$).

[4] Of course one could obtain a similar steady state also based on an imposed power profile, for instance computed using a Monte Carlo code or an external deterministic code.

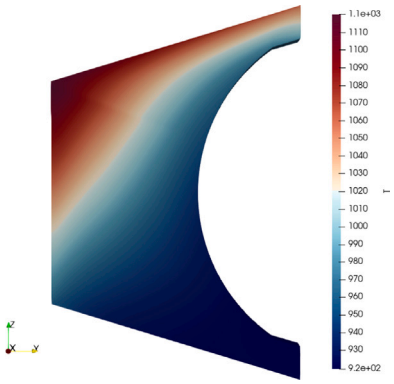

Fig. 7. Temperature distribution for the 2-D geometry.

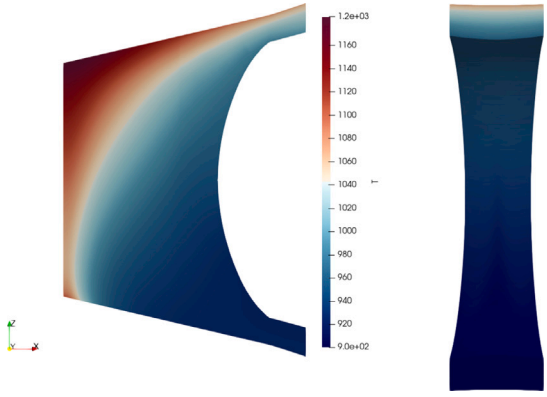

Fig. 8. Temperature distribution for the 3-D geometry.

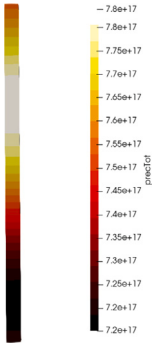

Fig. 9. Total precursors distributions for the 1-D geometry.

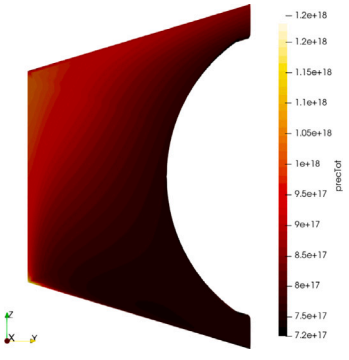

Fig. 10. Total precursors distributions for the 2-D geometry.

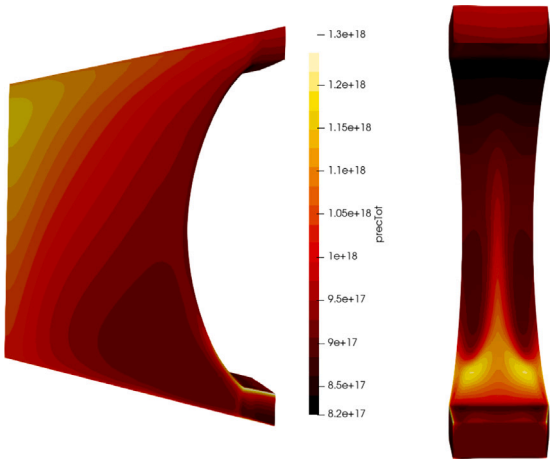

Fig. 11. Total precursors distribution for the 3-D geometry.

predicted precursors behavior in the different geometries and on its impact on the behavior of the reactor. As a reminder, the variation of β_{circ} with flow rate is an important quantity in circulating system, as it determines the amount of reactivity change during a transient that involves a changing flow field, such as a pump start up or a loss of flow accident.

The circulating delayed neutron fraction extends the concept of effective delayed neutron fraction and it aims at describing the effectiveness of delayed neutrons in circulating conditions. Its value has been estimated in this work based on the standard definition (see for instance (Aufiero et al., 2014a; Lapenta et al., 2001)):

$$\beta_{circ,i} = \frac{\int_V \sum_{g=1}^{G} \phi_g^* \chi_{d,g} \lambda_i C_i dV}{\int_V \left(\sum_{g=1}^{G} \phi_g^* \chi_{d,g} \sum_{k=1}^{R} \lambda_k C_k + \sum_{g=1}^{G} \phi_g^* \chi_{p,g} \sum_{g'=1}^{G} \phi_{g'} (\nu \Sigma_f)'_g \right) dV} \tag{23}$$

Another way some authors have employed to estimate β_{circ} in lumped-parameter codes is to use a simple analytical formula based on in-core (τ_c) and ex-core (τ_e) transit times (Cammi et al., 2012):

$$\beta_{circ,i}^{0D} = \frac{\beta_{eff,i}}{1 + \frac{1 - e^{-\lambda_i \tau_e}}{\lambda_i \tau_c}} \tag{24}$$

Fig. 12 shows the results obtained for the 3 geometries using Eq. (23), as well as using Eq. (24) (case named 0D in the figure). β_{circ} decreases with flow rate because of the increased number of precursors decaying outside of the core, or in low-importance regions towards the top of the core. The variation is smaller for the 0-D case, which can be ascribed to the lack of precursors weighting: a 0-D case cannot predict the effect of precursors accumulating in low-importance regions. For the same reason, the 2-D and 3-D cases show the steepest decrease of β_{circ} with flow rate. At low velocities, β_{circ} tends to converge to the β_{eff}. The fact that the 0-D and 3-D approaches give the same value at low velocities is a trivial consequence of employing in Eq. (24) the β_{eff} of the 3-D case. The similarity between 1-D and 3-D models at low velocities is instead associated with a compensation of errors. This is evident from Fig. 13, which shows that the 1-D approach overestimates the contribution to β_{circ} of slow-decaying precursors and underestimates that of fast-decaying precursors. It is interesting to observe how the 2-D model represents the outlier in the group. In this case, there are no compensation of errors among different precursors groups and the 2-D model suffers from the full effect of dimensionality vs the 3-D model, including different velocities and average residence times in the core, different turbulent diffusivity, slightly different neutron spectra, etc.

Fig. 13 also provides indication that the β_{circ} features strong non-linearities with respect to the flow rate. A good example is given

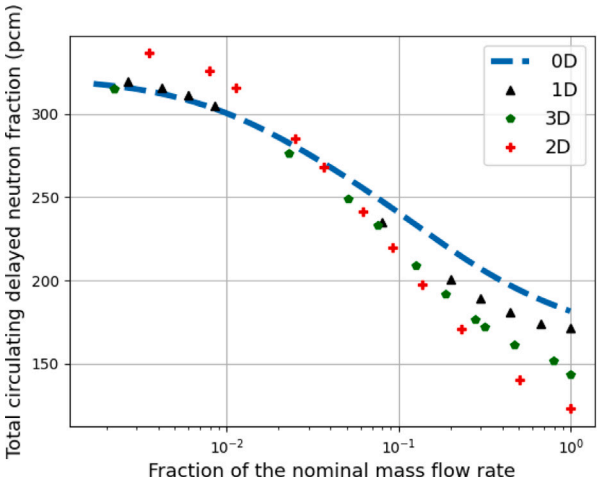

Fig. 12. Circulating delayed neutron fraction calculated based on a diffusion model for both forward and adjoint neutron flux, and well as by Eq. (24).

by group 1, where the 2-D and 3-D models start diverging at high flow rates, with the 3-D case that displays increase of β_{circ}. Although surprising at first sight, this behavior is a consequence of an increasing jet-effect from the core inlet, which generates larger low-velocity areas and a better retention of precursors.

Differences are found also for the groups that are only mildly affected by the flow, such as groups 7 and 8. The differences in this case can be ascribed to space-energy effects. The effective delayed neutron fraction for the 8th group is about 10% higher than the physical fraction for the 2-D model and 5% higher for the 3-D. This effect is completely absent in the 1-D case.

5. Transient results

Two transients have been used in this paper to investigate the effect of model dimensionality on the MSFR predicted behavior, namely: an unprotected transient over-power; and an unprotected loss of flow. The models and modeling choices described in Section 3 are employed and the diffusion approach applied on the 3-D geometry is used as a reference case. The cases where a uniform power density is assumed are referred to as *PK uniform*, whereas the point-kinetics cases informed by steady-state diffusion results are referred to as *PK*.

It is worth noting that, in MSRs, the effect of both a reactivity insertion and flow rate reduction are strongly affected by the state of the system previous to the perturbation since:

- the margin to prompt criticality depends on β_{circ};
- a lower β_{circ} implies a higher reactivity increment when the flow rate decreases.

In order to make meaningful comparisons among models, their steady-state β_{circ} prior to the transient has been calculated and reported in Table 6. For a diffusion-based evaluation, the formula (23) is used, whereas, for the modified point kinetics model described in Section 2.2, β_{circ} is calculated as:

$$\beta_{circ,i} = \frac{\Lambda \lambda_i \hat{C}_i}{P(0)} = \frac{\Lambda}{P(0)} \frac{\int_V W(r)\lambda_i \tilde{c}_i(r) dV}{\int_V W(r) S(r) dV} \tag{25}$$

Table 6 shows that a diffusion-informed model with spatial treatment of precursors provides reasonably accurate predictions of β_{circ}, while uniform power and neutron importance lead to a significant overestimation of this essential parameter. With diffusion-based, or diffusion-informed calculations, also the dimensionality contribute significantly to differences among models. In particular, the 1-D model significantly overestimates the β_{circ}, which will result in non-conservative predictions for reactivity-initiated transients. Since the flow rate is the same in the three cases, we hypothesize the reason for this is the accumulation of precursors in low-importance regions of the 2-D and 3-D geometries (see Figs. 10 and 11).

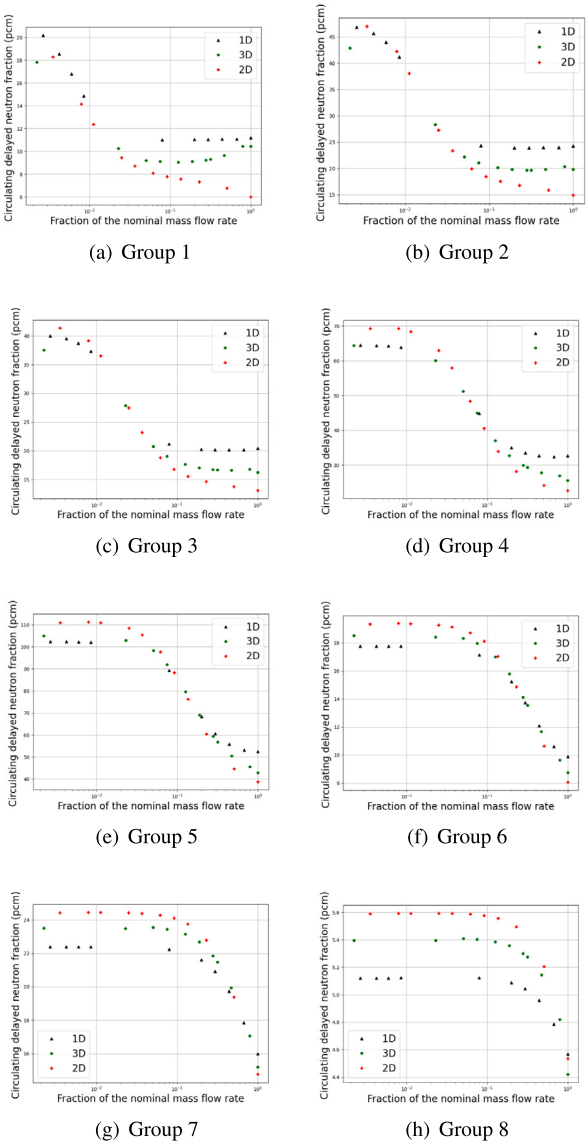

Fig. 13. Circulating delayed neutron fraction for each delayed neutron group.

Table 6
Circulating delayed neutron fraction for different models and in the three geometries.

Circulating delayed neutron fraction (pcm)	3D	2D	1D
Diffusion-based	137.0	122.9	171.6
Diffusion informed point-kinetics	142.3	112.8	169.74
Point kinetics with uniform power density and neutron importance	193.6	184.0	193.6

5.1. Unprotected transient overpower

A reactivity initiated accident is simulated for simplicity as a step-wise reactivity insertion. In the MSFR, no control rods are currently foreseen, but an increase in reactivity may occur due to failure of the gas sparging system or an accidental insertion of fissile material. A reactivity insertion equal to 30 pcm was assumed for all cases.

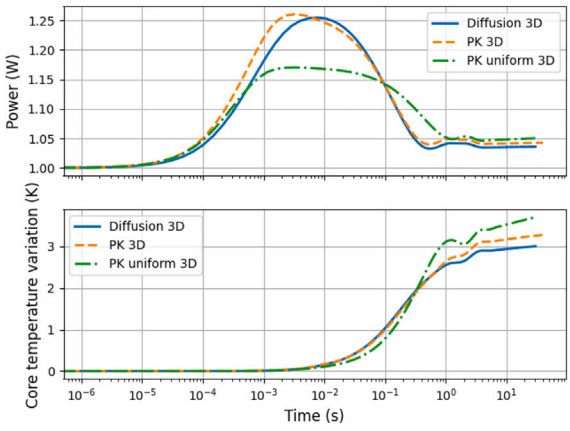

Fig. 14. Simulation of a transient overpower in the 3D geometry.

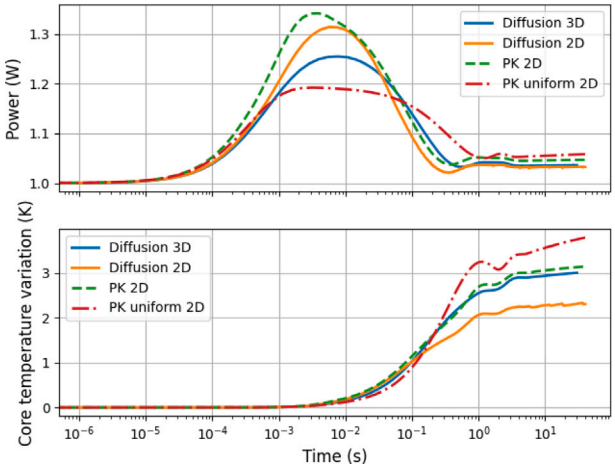

Fig. 15. Simulation of a transient overpower in the 2D geometry.

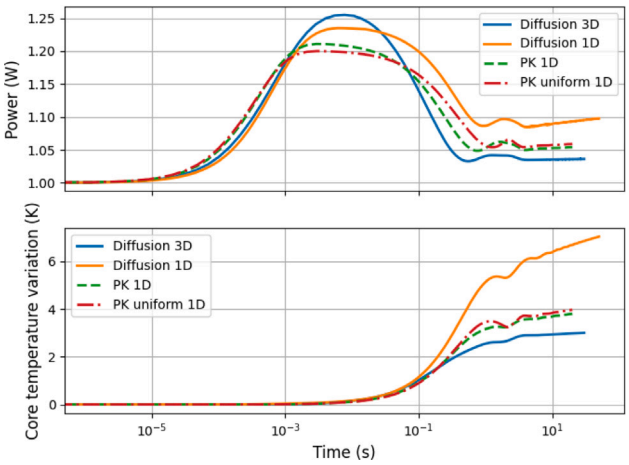

Fig. 16. Simulation of a transient overpower in the 1D geometry.

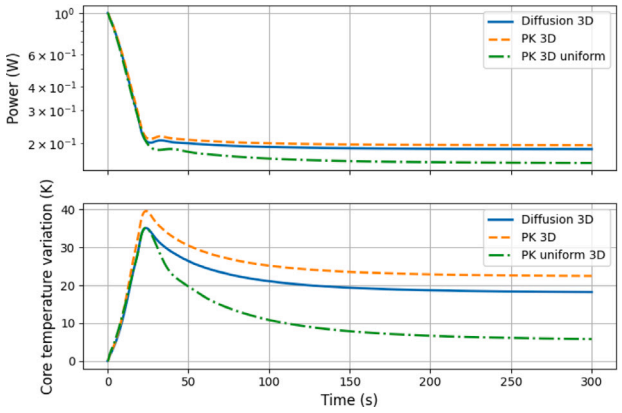

Fig. 17. Simulation of a loss of flow in the 3-D geometry.

Fig. 14 shows that, in a 3-D simulation, a diffusion-informed point-kinetics model can give results that are very close to a diffusion model, while a more simplified point-kinetics model with uniform power density and neutron importance can lead to a non-negligible underestimation of the peak power (~6% on peak absolute power, and ~60% on peak relative power). This is consistent with the results reported in Table 6. It should be mentioned that the assumption of a uniform power density also implies starting from a different steady state compared to the one discussed in Section 4.

The results reported in Figs. 15 and 16 provide a comparison between the 3-D case, which is assumed as reference, and the lower dimensional geometries (2-D and 1-D). In the 2-D geometry, the diffusion model overestimates the peak power, due to a lower margin from prompt criticality (see Table 6). The point-kinetics model overestimates the power even further compared to the diffusion model on the same geometry, but resembles quite closely to the diffusion model. As in the 3-D geometry, the case with a uniform power density fails at giving an accurate power evolution of the transient.

For the 1-D case, the diffusion model gives results that are less accurate than point kinetics after the peak. This occurs because the one-dimensional geometry is unable to correctly reproduce the effect of density feedback, as discussed in Section 3, which results in a higher core temperature variation to counterbalance the reactivity insertion. The point-kinetics cases are instead fed with point-kinetics parameters that are generated with a 3-D geometry. Therefore the discrepancy between the 1-D geometry (with point-kinetics) and the 3D case are mostly due to the thermal-hydraulics modeling. It is worth noting that assuming a uniform power density in the 1-D model does not lead to significantly different results compared to a diffusion-informed point-kinetics model.

5.2. Unprotected loss of flow

A loss of flow scenario normally leads to a significant increase in the temperature of the hot leg, and to a similar decrease in temperature in the cold leg. In liquid fueled reactors, the loss of flow is also related to reactivity effects due to the higher retention of precursors in the core as a result of the decreased flow rate.

The loss of flow is modeled in this paper as an exponential decrease of the momentum source in the pump, down to 10% of the nominal value. The results are given in Figs. 17–20.

As a result of the increased power-to-flow ratio, the core average temperature increases during the first 20 seconds. Subsequently, the core average temperature decreases and reaches a steady state. The core average temperature at the end of the transient compensates the reactivity increase due to the increased delayed neutrons retention in the core. Therefore, the core temperature variation at the end of the transient reflects the variation of β_{circ}, as well as potentially different temperature patterns in core.

In 3-D, the point-kinetics models resembles the reference diffusion solution during the initial temperature rise. This is due to the fact that the feedback coefficients have been calculated based on the 3-D diffusion model. In the longer term, the different predictions in β_{circ} tend to dominate, with the point-kinetics model with uniform

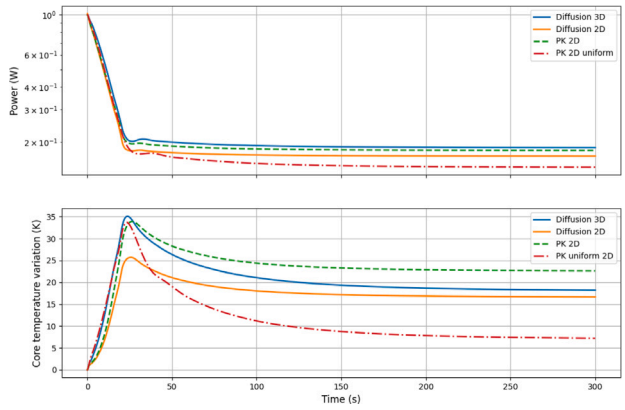

Fig. 18. Simulation of a loss of flow in the 2-D geometry.

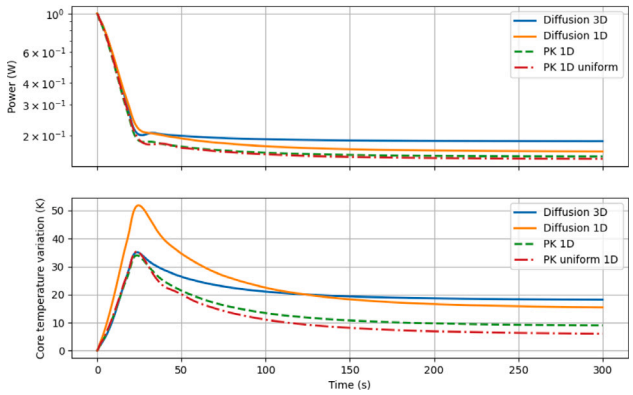

Fig. 19. Simulation of a loss of flow in the 1-D geometry.

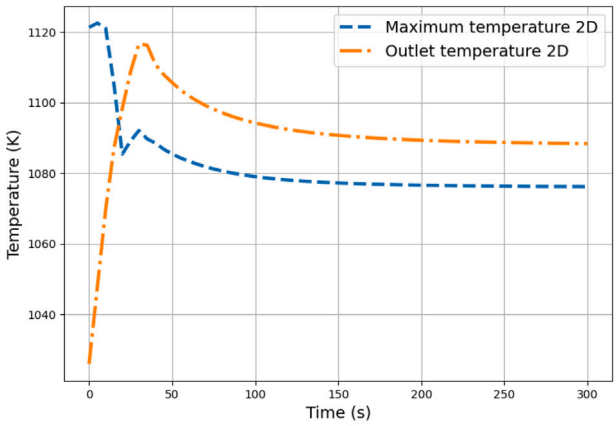

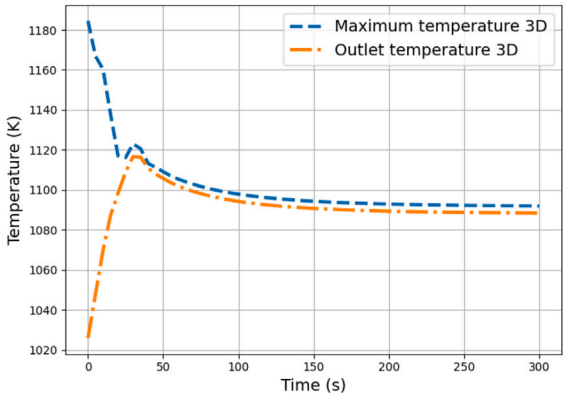

Fig. 20. Maximum and core outlet temperature for the 2-D and 3-D geometries during a loss of flow. The 1-D case has been omitted as core outlet and maximum temperature coincides.

power and neutron importance that heavily underestimates temperatures and power. The diffusion-informed point-kinetics model slightly overestimates temperature variations. We hypothesize that this is due to slight differences in the temperature pattern at lower velocities, whose impact on reactivity can be captured by spatial neutronics, but not by point-kinetics.

In the 2-D geometry, we observe similar differences between diffusion and point-kinetics, as well as the same underestimation of power and temperatures for the case with uniform power and neutron importance. We also observe that a diffusion calculation in 2-D can give significantly different results compared to a 3-D case.

In the 1-D geometry, we observe a smaller impact of power and neutron importance shapes that is consistent with results for the transient overpower. However, in this case, both results tend to be quite far from the reference 3-D diffusion result. We also observe the same outlier behavior for the diffusion model, which is again due to the missing reactivity contribution of density variations.

A loss-of-flow scenario allows to highlight the effect of a changing flow pattern on local figures of merit. As an example, one might be tempted to use the core outlet temperature as an indication of the maximum temperature in the core. Fig. 20 shows instead that maximum temperatures behave very differently with respect to outlet temperatures. They start off from a steady-state value that mainly depends on the existence, positioning, and size of low-velocity regions, and gradually approach the behavior of the outlet temperature, but with a significant offset. The results are also very sensitive to the dimensionality of the model, with the final offset that is positive for the 3-D case, and negative for the 2-D case. One should notice that the 1-D and 2-D cases are significantly non conservative.

6. Discussion and conclusions

A study on the effects of modeling assumptions on the predicted behavior of fast-spectrum MSRs has been carried out. Our results suggest that safety analyses should include the use a 3-D representation of the reactor core. Simulations with lower dimensionality entail significant approximations that are difficult to correct via calibration and that may raise concerns about the validity of the safety analysis. In particular, model dimensionality significantly affects:

- **Local temperatures**, with the risk of under-predicting maximum temperatures; of not predicting salt freezing; or even of not predicting a flow-detachment situation with the risk of extremely high temperatures (see Fiorina et al., 2014).
- **Temperature distributions and neutron importance**, with the risk of significantly over-predicting feedback coefficients.
- **Precursors distributions and neutron importance**, with the risk of significant approximations in the evaluation of β_{circ}. This would affect control rod design and all predictions about reactivity initiated accidents. In addition, in MSRs, the difference between β_{eff} and β_{circ} also determines the reactivity insertion in case of a loss of low, and ultimately the core temperatures at the end of the transient.

The findings of this paper should serve as a warning regarding the utilization of low-dimensionality model. These include 1-D models, but also 2-D axial-symmetric models that are often employed within the community. 2-D models inevitably result in significant geometric approximations that in turn can generate questionable predictions in

terms of flow patterns, recirculation/stagnation regions, and ultimately reactor behavior and safety. Calibrating a low-dimensional model on a 3-D steady-state simulation may not be sufficient, or may be difficult to justify to a licensing authority, since flow patterns tend to significantly change for different flow rates. For instance, maximum core temperatures have been shown to behave differently than core outlet temperatures in case of a loss of flow.

We would like to point out that a 3-D model of a reactor loop required a few GB of RAM and several minutes to few hours (for the longest transients) to run on a personal computer. A full-core 3-D model may require a more capable workstation, but likely not a cluster. A 3-D model based on Large Eddy Simulation instead of Reynolds Average Navier Stokes may require a small cluster. Overall, we believe that these figures fully fall into what analysts today have access to, and that simulations lasting up to several hours are largely acceptable within the context of a safety analysis.

Although we believe that the exclusive use of 1-D and 2-D models is hard to justify today for safety-related studies, they remain valuable tools for reactor design, control-oriented studies, uncertainty quantification and data assimilation, as well as fundamental studies on the MSR behavior. However, proper calibration of these models is needed, and the user should be aware that changing flow patterns could jeopardize model calibration.

In terms of dimensionality of the neutronics model, we observe that point-kinetics models can provide accurate results as long as: precursors are treated spatially; the model is provided with correct distributions for power and neutron importance; feedback coefficients are calculated based on representative temperature distributions and neutron importance. Power/importance distribution and kinetic parameters should ideally be obtained from spatial neutron kinetics calculations, which would point in the direction of using spatial kinetics directly in the transient analysis. However, we recognize that one may find it beneficial to obtain power/importance distribution and kinetic parameters using an external tool. For instance, GeN-Foam allows for a two-way coupling with the Serpent Monte Carlo code.[5] One can run a Serpent calculations on the OpenFOAM mesh (no need for a separate, combinatorial or CAD geometry) (Fiorina et al., 2019); use the resulting flux, power distributions, β_{eff} and generation time as inputs to the point-kinetics model; and perturb the power to obtain reactivity feedback coefficients. This approach has the merit of bypassing the time-consuming and error-prone step of few-groups cross-section generation.

As a last remark, we observe that some spatial effects like peak local temperatures are expected to be less significant in reactor designs with lower power densities. On the other hand, other effects not simulated in this work are suspected to make dimensional effects even more important. A good example is helium sparging, whose effect on reactivity is strongly space dependent, and whose distribution is strongly dependent on the flow pattern.

CRediT authorship contribution statement

Nahom Habtemariam: Methodology, Software, Writing – original draft, Editing. **Carlo Fiorina:** Conceptualization, Software, Writing – original draft, Editing. **Stefano Lorenzi:** Conceptualization, Writing – original draft, Editing. **Antonio Cammi:** Supervision.

Declaration of competing interest

The authors declare that they have no known competing financial interests or personal relationships that could have appeared to influence the work reported in this paper.

[5] More precisely, the Serpent multi-physics coupling allows for two-ways coupling with any OpenFOAM-based solver.

Data availability

Data will be made available on request.

References

Aufiero, M., Brovchenko, M., Cammi, A., Clifford, I., Geoffroy, O., Heuer, D., Laureau, A., Losa, M., Luzzi, L., Merle-Lucotte, E., Ricotti, M.E., Rouch, H., 2014a. Calculating the effective delayed neutron fraction in the molten salt fast reactor: Analytical, deterministic and Monte Carlo approaches. Ann. Nucl. Energy 65, 78–90. http://dx.doi.org/10.1016/j.anucene.2013.10.015.

Aufiero, M., Cammi, A., Geoffroy, O., Losa, M., Luzzi, L., Ricotti, M.E., Rouch, H., 2014b. Development of an OpenFOAM model for the Molten Salt Fast Reactor transient analysis. Chem. Eng. Sci. 111, 390–401. http://dx.doi.org/10.1016/j.ces.2014.03.003, URL https://www.sciencedirect.com/science/article/pii/S0009250914001146.

Ball, S.J., Kerlin, T.W., 1965. Stability analysis of the molten salt reactor experiment.

Bell, G.I., Glasstone, S., 1970. Nuclear Reactor Theory. Krieger Publishing Company.

Brovchenko, M., Kloosterman, J.-L., Luzzi, L., Merle, E., Heuer, D., Laureau, A., Feynberg, O., Ignatiev, V., Aufiero, M., Cammi, A., et al., 2019. Neutronic benchmark of the molten salt fast reactor in the frame of the EVOL and MARS collaborative projects. Eur. Phys. JN 5, 2.

Cammi, A., Fiorina, C., Guerrieri, C., Luzzi, L., 2012. Dimensional effects in the modelling of MSR dynamics: Moving on from simplified schemes of analysis to a multi-physics modelling approach. Nucl. Eng. Des. 246, 12–26. http://dx.doi.org/10.1016/j.nucengdes.2011.08.002, URL https://www.sciencedirect.com/science/article/pii/S0029549311006273.

Cervi, E., Lorenzi, S., Cammi, A., Luzzi, L., 2019. Development of an SP3 neutron transport solver for the analysis of the molten salt fast reactor. Nucl. Eng. Des. 346, 209–219. http://dx.doi.org/10.1016/j.nucengdes.2019.03.001, URL https://www.sciencedirect.com/science/article/pii/S0029549319300354.

Fiorina, C., 2022. The GeN-foam multiphysics solver: A status update. In: International Conference on Physics of Reactors 2022 (PHYSOR 2022), Pittsburgh, PA, May 15-20.

Fiorina, C., Aufiero, M., Cammi, A., Franceschini, F., Krepel, J., Luzzi, L., Mikityuk, K., Ricotti, M.E., 2013. Investigation of the MSFR core physics and fuel cycle characteristics. Prog. Nucl. Energy 68, 153–168. http://dx.doi.org/10.1016/j.pnucene.2013.06.006, URL https://www.sciencedirect.com/science/article/pii/S0149197013001236.

Fiorina, C., Aufiero, M., Cammi, A., Guerrieri, C., Krepel, J., Luzzi, L., Mikityuk, K., Ricotti, M.E., 2012. Analysis of the MSFR Core Neutronics Adopting Different Neutron Transport Models. In: Volume 5: Fusion Engineering; Student Paper Competition; Design Basis and beyond Design Basis Events; Simple and Combined Cycles. In: International Conference on Nuclear Engineering, pp. 219–228. http://dx.doi.org/10.1115/ICONE20-POWER2012-54519.

Fiorina, C., Clifford, I., Aufiero, M., Mikityuk, K., 2015. GeN-foam: a novel [openfoam]® based multi-physics solver for 2D/3D transient analysis of nuclear reactors. Nucl. Eng. Des. 294, 24–37. http://dx.doi.org/10.1016/j.nucengdes.2015.05.035.

Fiorina, C., Kerkar, N., Mikityuk, K., Rubiolo, P., Pautz, A., 2016. Development and verification of the neutron diffusion solver for the GeN-foam multi-physics platform. Ann. Nucl. Energy 96, 212–222. http://dx.doi.org/10.1016/j.anucene.2016.05.023.

Fiorina, C., Lathouwers, D., Aufiero, M., Cammi, A., Guerrieri, C., Kloosterman, J.L., Luzzi, L., Ricotti, M.E., 2014. Modelling and analysis of the MSFR transient behaviour. Ann. Nucl. Energy 64, 485–498. http://dx.doi.org/10.1016/j.anucene.2013.08.003.

Fiorina, C., Radman, S., Koc, M.-Z., Pautz, A., 2019. Detailed modelling of the expansion reactivity feedback in fast reactors using OpenFOAM. In: M&C 2019, Portland, OR, August 25-29.

Harvill, R.C., Lane, J.W., Link, J.M., Claybrook, S.W., George, T.L., Kindred, T., 2022. Steady-State and Transient Benchmarks of GOTHIC to the Molten Salt Reactor Experiment. Nucl. Technol. 208, 70–99. http://dx.doi.org/10.1080/00295450.2021.1884491.

Křepel, J., Rohde, U., Grundmann, U., Weiss, F.-P., 2007. DYN3D-MSR spatial dynamics code for molten salt reactors. Ann. Nucl. Energy 34 (6), 449–462. http://dx.doi.org/10.1016/j.anucene.2006.12.011, URL https://www.sciencedirect.com/science/article/pii/S0306454907000527.

Lapenta, G., Mattioda, F., Ravetto, P., 2001. Point kinetic model for fluid fuel systems. Ann. Nucl. Energy 28 (17), 1759–1772. http://dx.doi.org/10.1016/S0306-4549(01)00012-3.

Lindsay, A., Ridley, G., Rykhlevskii, A., Huff, K., 2018. Introduction to Moltres: An application for simulation of Molten Salt Reactors. Ann. Nucl. Energy 114, 530–540. http://dx.doi.org/10.1016/j.anucene.2017.12.025, URL https://www.sciencedirect.com/science/article/pii/S0306454917304760.

Mattioli, A., Fiorina, C., Lorenzi, S., Cammi, A., 2021. Derivation and implementation in OpenFOAM of a point-kinetics model for Molten Salt Reactors. In: ANS Winter Meeting 2021.

Tiberga, M., Lathouwers, D., Kloosterman, J.L., 2020. A multi-physics solver for liquid-fueled fast systems based on the discontinuous Galerkin FEM discretization. Prog. Nucl. Energy 127, 103427. http://dx.doi.org/10.1016/j.pnucene.2020.103427, URL https://www.sciencedirect.com/science/article/pii/S0149197020301797.

Todreas, N.E., Kazimi, M.S., Massoud, M., 2021. Nuclear Systems Volume II: Elements of Thermal Hydraulic Design. CRC Press.

Yang, G., Jaradat, M.K., Sik Yang, W., Lee, C., 2022. Development of coupled PROTEUS-NODAL and SAM code system for multiphysics analysis of molten salt reactors. Ann. Nucl. Energy 168, 108889. http://dx.doi.org/10.1016/j.anucene.2021.108889, URL https://www.sciencedirect.com/science/article/pii/S0306454921007660.

Zanetti, M., Cammi, A., Fiorina, C., Luzzi, L., 2015. A geometric multiscale modelling approach to the analysis of MSR plant dynamics. Prog. Nucl. Energy 83, 82–98. http://dx.doi.org/10.1016/j.pnucene.2015.02.014, URL https://www.sciencedirect.com/science/article/pii/S0149197015000487.